Acta Geologica Sinica (English Edition), 2019, 93(6): 1900–1908

Oxygen Fugacity and Water Activity during Thermal Peak and Retrogression of Granulites around the Sarvapuram Area, Karimnagar Granulite Terrane, Andhra Pradesh, India

P. Chandra SINGH[1, 2, *] and D. PRAKASH[2]

[1] *Department of Earth Sciences, Indian Institute of Technology, Powai, Mumbai, 400076, India*
[2] *Centre of Advanced Study in Geology, Banaras Hindu University, Varanasi, 221005, India*

Abstract: The investigated area around Sarvapuram represents a part of the Karimnagar granulite terrane of the Eastern Dharwar Craton, India. Garnet–bearing gneiss is hosted as enclaves, pods within granite gneiss and charnockite. It is largely made up of garnet, orthopyroxene, cordierite, biotite, plagioclase, K–feldspar, sillimanite and quartz. The peak metamorphic stage is represented by the equilibrium mineral assemblage i.e. garnet, orthopyroxene, cordierite, biotite, plagioclase, sillimanite and quartz. Breakdown of the garnet as well as preservation of the orthopyroxene–cordierite symplectite, formation of cordierite with the consumption of the garnet + sillimanite + quartz represents the decompressional event. The thermobarometric calculations suggest a retrograde *P–T* path with a substantial decompression of c. 3.0 kbar. The water activity (X_{H2O}) conditions obtained with the winTWQ program for core and symplectite compositions from garnet–bearing gneiss are 0.07–0.14 and 0.11–0.16 respectively. The quantitative estimation of oxygen fugacity in garnet–bearing gneiss reveal log fO_2 values ranging from −11.38 to −14.05. This high oxidation state could be one of the reasons that account for the absence of graphite in these rocks.

Key words: metamorphic conditions, oxygen fugacity, water activity, garnet–bearing gneisses, Karimnagar granulite terrane, India

Citation: Singh and Prakash et al., 2019. Oxygen Fugacity and Water Activity during Thermal Peak and Retrogression of Granulites around the Sarvapuram Area, Karimnagar Granulite Terrane, Andhra Pradesh, India. Acta Geologica Sinica (English Edition), 93(6): 1900–1908. DOI: 10.1111/1755-6724.13817

1 Introduction

Metamorphic rocks are seen as a living witness to the geodynamic processes that took place throughout Earth's history and tell us primarily about the pressure or depth (*P*), temperature (*T*), activity of the fluid phases (*X*), and time (*t*) of their journey. The generalized *P–T–X* loop is a composite diagram which includes (a) entrapped mineral inclusions in poikiloblasts (b) the peak (*P–T*) conditions from geothermobarometry (c) retrograde path from the reset mineral equilibria and (d) realm of entrapment of fluid inclusions. In the last two decades, a considerable number of experimental and theoretical works on minerals have been undertaken in order to understand the thermodynamic properties of minerals and their solid solutions. These data are highly useful, particularly for high grade metamorphic rocks, where nothing else helps in contemplating the dynamic evolution of Earth's lower crust. The remarkable internally consistent data set and continuously improving activity models of mineral phases have provided precise and accurate *P–T–X* estimates over the earlier crude methods. Therefore, more recently the *P–T–X* paths have been the subject of a large number of studies and excellent reviews have been given by Bohlen (1987, 1991), Bohlen and Mezger (1989), Dasgupta (1995), Gerya (2014), Harley (1989), Mohan and Jayananda (1999), Prakash et al. (2012, 2015), Sizova et al. (2014), Spear (1992, 1993) and Zhai et al. (2005).

Granulites are broadly accepted to constitute the deeper part of the continents and have an important bearing on understanding the petrogenesis of the crust. Besides the physical conditions, fluid and the redox potential (oxidation state) play important roles in the recrystallization and growth of mineral phases during granulite facies metamorphism. In the context of the Indian peninsula, although only a few attempts have been made to suggest the activity of the fluid and oxidation condition from the granulite localities of Eastern Ghats Mobile Belt and Southern Granulite terrane e.g. Anakapalle (Lal et al., 1998), and Kodaikanal Massif (Prakash, 2000), until now no attempt had been made to quantify the activity of the fluid and oxidation condition in the Karimnagar granulites. In the present paper, we describe the summary of textural relationship, mineral chemistry and *P–T–X* and oxidation condition of the garnet–bearing gneiss from the Sarvapuram area of the Karimnagar granulite terrane.

2 Geological Background

The Karimnagar granulite terrane (KGT) is an integral part of the Eastern Dharwar Craton (EDC) and extends along a NW–SE trend in the Telangana state (Fig.1a). It is

* Corresponding author. E-mail: pcsinghgeo21@gmail.com

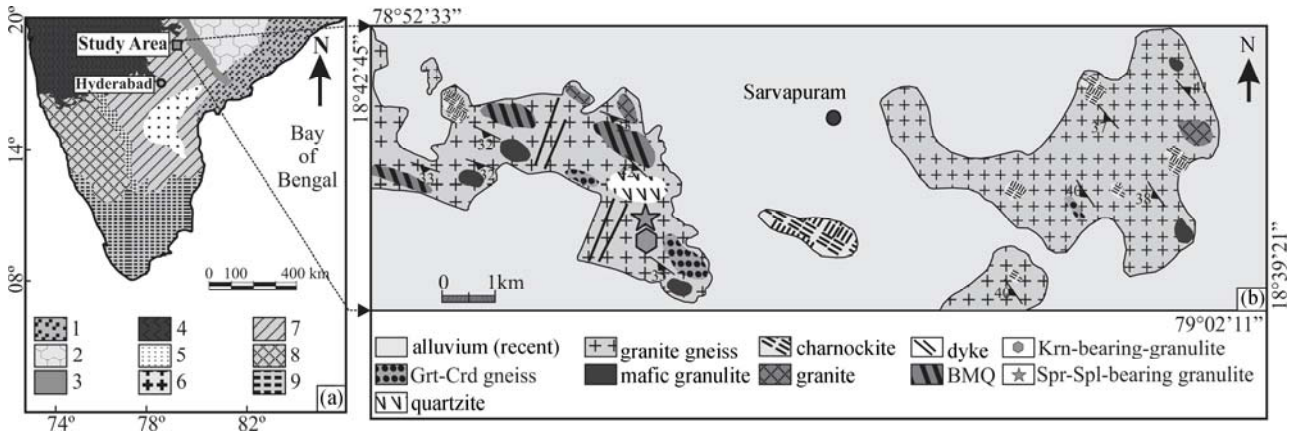

Fig. 1. (a) Geological and tectonic map of southern India, after Crowe, et al. (2003); Mishra, et al. (2000); Naqvi and Rogers (1987); Prakash, et al. (2017).
Legends represent the following regions: 1–Eastern Ghat Mobile Belt; 2–Bastar craton; 3–Godawari graben; 4–Deccan trap; 5–Cuddapah Basin; 6–Closepet Granite; 7–Eastern Dharwar craton; 8–Western Dharwar Craton; 9–Southern Granulite Terrane. (b) Geological map of the area around Sarvapuram.

situated along the southern flank of the Godavari graben which separates the Dharwar and Bastar cratons (Fig. 1a). The KGT rose to prominence after the discovery of quartz–absent sapphirine–spinel–bearing granulites and garnet–bearing gneisses from different localities viz. Malial, Podur, Namlekonda, Kalleda, Narella, Kottur etc. (Patel et al., 2010; Prakash et al., 2011, 2013a, b, 2017; Prakash and Sharma, 2008, 2011; Prakash and Singh, 2014; Sarbajna et al., 2013; Sharma and Prakash, 2008). The EDC shows the gradual increase in the grade of metamorphism, from north to south, from greenschist to amphibolite and ultimately granulite facies (Pichamuthu, 1965; Raase et al., 1986; Raith et al., 1982) and may be a result of single or multiple thermal events. According to Mahabaleswar et al. (1995), Maibam et al. (2011) and Peucat et al. (2013), the Dharwar Craton was affected by a series of high–grade regional metamorphic events. Normally, the lowest grade of metamorphic rocks should be present towards the furthest north of the greenschist facies, but the presence of high grade granulite facies rocks of KGT makes the area one of special interest. So far, it has remained unclear as to whether or not the granulite–facies metamorphism in KGT is related to the Southern Granulite Belt.

The study area constitutes a part of the KGT and is predominantly composed of granite gneiss, charnockite and granite (Fig. 1b). The granulite facies rocks e.g. charnockite, basic granulite, gneiss and quartz–free granulite are found as enclaves within granite gneiss and charnockite (Fig. 1b). In addition, banded magnetite quartzite, metadolerites, quartzite and altered ultramafic rocks are other important rock types present. Mostly, outcrops occur as isolated hillocks or detached blocks, which prevents a comprehensive structural analysis, although measurement on foliations in gneisses and schists suggests the general strike lies along NW–SE with a variation from NNW–SSE to WNW–ESE with moderate to steep dips either in east or west directions. The garnet–bearing gneisses are extensively exposed near Sarvapuram and utilized in the *P–T* estimation, activity of water as well as oxygen fugacity conditions. Three phases of deformation have been constrained in the gneissic units i.e., garnet–bearing (garnet–cordierite gneiss) and garnet–absent gneiss (biotite–cordierite gneiss), of the study area. The first deformation event produced a NE–SW trending tight isoclinal fold. The prominent second phase of deformation is characterized by tight upright-to-reclined folds that strike NW–SE, deforming earlier fabrics. It defines the dominant structural trend in the rocks and delineates the general strike in the area. The third deformation event yielded large open folds with steeply plunging axes.

3 Petrography and Mineral Chemistry

The gneisses are dark in colour, medium (2–5 mm) to coarse–grained (>5 mm), hard and compact. Although megascopically foliation is not clearly visible, biotite and rarely orthopyroxene show preferred orientation at a microscopic level. Among the various rock units observed in the study area, two representative samples of garnet-bearing gneiss (samples 14–4B and 14–6F) were selected for detailed petrological investigation. Although both samples were petrographically similar and retain very well–preserved mineral parageneses, they differ in the grain size and mineral chemical data of each phase, as well as 14–6F lacking the mineral sillimanite.

Detailed instrument conditions for electron probe microanalysis (EPMA) is discussed in Prakash et al. (2017). Representative mineral chemistry data acquired from the EPMA is reported in Tables 1 and 2.

In both samples, garnet occurs as medium to coarse-grained xenoblastic to subidioblastic crystals (Fig. 2a, d, e). In general, coarse–grained garnet contains variable size inclusions of biotite, quartz, feldspars, magnetite, ilmenite, ± sillimanite may occur. However, medium–grained, idioblastic or subidioblastic garnets are inclusion– free (Fig. 2b–c). These are relatively rich in the almandine component (0.53–0.72) rather than pyrope (0.19–0.39). The grossular, spessartine and andradite contents are very low, varying up to 0.04, 0.05 and 0.02 respectively (Table 1).

Orthopyroxene (Opx) crystals from both the samples

Table 1 Representative microprobe analyses and structural formulae of garnet, orthopyroxene and cordierite

Sample	14-4B	14-4B	14-6F	14-6F	14-4B	14-4B	14-6F	14-6F	14-4B	14-4B	14-6F	14-6F
minerals	Grt_p	Grt_s	Grt_p	Grt_s	Opx_m	Opx_s	Opx_m	Opx_s	Cd_m	Cd_s	Cd_m	Cd_s
wt%												
SiO_2	38.51	37.18	38.62	38.27	51.47	51.36	50.12	48.80	48.62	48.28	48.53	48.85
TiO_2	0.02	0.05	0.10	0.00	0.07	0.09	0.11	0.08	0.00	0.00	0.02	0.05
Al_2O_3	21.52	21.09	21.44	21.66	3.59	3.62	4.05	5.03	32.21	32.64	32.24	32.61
Cr_2O_3	0.17	0.14	0.23	0.19	0.15	0.18	0.37	0.34	0.00	0.00	0.00	0.02
FeO*	25.46	32.46	32.06	30.01	21.60	26.09	26.58	33.03	4.99	4.22	7.27	5.42
MnO	1.88	2.21	0.00	0.38	1.13	1.18	0.26	0.34	0.11	0.16	0.05	0.01
MgO	10.28	4.72	6.88	8.51	21.61	16.99	17.40	12.44	10.30	10.30	8.80	9.74
CaO	1.48	1.38	0.15	0.17	0.15	0.18	0.00	0.00	0.02	0.03	0.01	0.00
Na_2O	0.00	0.00	0.00	0.01	0.03	0.01	0.02	0.00	0.06	0.05	0.02	0.03
K_2O	0.00	0.00	0.00	0.00	0.01	0.01	0.03	0.00	0.00	0.05	0.02	0.00
Total	99.32	99.23	99.48	99.20	99.81	99.71	98.94	100.06	96.31	95.73	96.96	96.73
O Basis	12	12	12	12	6	6	6	6	18	18	18	18
Unit(p.f.u.)												
Si	2.980	2.986	3.033	2.995	1.918	1.953	1.922	1.908	5.033	5.012	5.039	5.038
Ti	0.001	0.003	0.006	0.000	0.002	0.003	0.003	0.002	0.000	0.000	0.002	0.004
Al	1.963	1.996	1.985	1.998	0.158	0.162	0.183	0.232	3.930	3.993	3.945	3.963
Cr	0.010	0.009	0.014	0.012	0.004	0.005	0.011	0.011	0.000	0.000	0.000	0.002
Fe^{2+}	1.601	2.174	2.106	1.964	0.673	0.837	0.857	1.088	0.432	0.366	0.631	0.467
Fe^{3+}	0.046	0.006	0.000	0.000	0.001	0.000	0.000	0.000	0.000	0.000	0.000	0.000
Mn	0.123	0.150	0.000	0.025	0.036	0.038	0.008	0.011	0.010	0.014	0.004	0.001
Mg	1.185	0.565	0.805	0.992	1.201	0.963	0.995	0.725	1.590	1.594	1.362	1.498
Ca	0.123	0.119	0.013	0.014	0.006	0.007	0.000	0.000	0.002	0.003	0.001	0.000
Na	0.000	0.000	0.000	0.002	0.002	0.001	0.001	0.000	0.012	0.010	0.004	0.006
K	0.000	0.000	0.000	0.000	0.000	0.000	0.001	0.000	0.000	0.007	0.003	0.000
X_{Mg}/ X_{An}/X_K	0.43	0.21	0.28	0.34	0.64	0.53	0.54	0.40	0.79	0.81	0.68	0.76

*Total iron as FeO; Fe^{2+} and Fe^{3+} are calculated by stoichiometric charge balance, X_{Mg}=Mg/ (Mg+Fe^{2+}), p–peak, s–symplectite, m–matrix.

Table 2 Representative microprobe analyses and structural formulae of biotite, plagioclase and K–feldspar

Sample	14-4B	14-4B	14-6F	14-6F	14-4B	14-4B	14-6F	14-6F	14-4B	14-4B	14-6F	14-6F
wt%												
Minerals	Bi_m	Bi_s	Bi_m	Bi_s	Pl_m	Pl_s	Pl_m	Pl_s	Kfs_m	Kfs_m	Kfs_m	Kfs_m
SiO_2	37.08	35.54	38.13	36.93	57.91	56.52	57.56	58.41	64.97	64.83	64.29	64.56
TiO_2	4.95	5.15	3.97	4.10	0.00	0.00	0.00	0.00	0.00	0.00	0.00	0.00
Al_2O_3	15.03	15.27	15.92	16.05	25.80	26.04	26.23	26.63	19.63	20.27	19.84	19.44
Cr_2O_3	0.00	0.00	0.32	0.67	0.00	0.00	0.00	0.00	0.02	0.01	0.01	0.01
FeO*	12.49	16.23	13.02	16.70	0.16	0.06	0.06	0.02	0.08	0.05	0.05	0.07
MnO	0.04	0.05	0.00	0.09	0.00	0.00	0.00	0.00	0.02	0.02	0.01	0.01
MgO	15.15	12.46	14.95	12.25	0.05	0.01	0.00	0.00	0.00	0.00	0.00	0.00
CaO	0.04	0.00	0.00	0.08	7.94	8.87	8.76	8.87	0.11	0.12	0.13	0.10
Na_2O	0.08	0.05	0.02	0.06	6.67	6.19	6.51	5.19	2.61	3.53	3.06	2.43
K_2O	9.53	9.51	9.65	9.49	0.16	0.13	0.13	0.09	12.14	10.79	11.51	12.45
Total	94.39	94.26	95.98	96.42	98.69	97.82	99.25	99.21	99.58	99.62	98.90	99.09
O Basis	22	22	22	22	6	6	6	6	6	6	6	6
Unit(p.f.u.)												
Si	5.533	5.425	5.589	5.501	2.622	2.588	2.597	2.618	2.968	2.947	2.953	2.968
Ti	0.556	0.591	0.438	0.459	0.000	0.000	0.000	0.000	0.000	0.000	0.000	0.000
Al	2.643	2.747	2.750	2.818	1.377	1.405	1.395	1.407	1.057	1.086	1.074	1.054
Cr	0.000	0.000	0.037	0.079	0.000	0.000	0.000	0.000	0.001	0.000	0.000	0.001
Fe^{2+}	1.558	2.072	1.596	2.080	0.006	0.002	0.002	0.001	0.003	0.002	0.002	0.003
Fe^{3+}	0.000	0.000	0.000	0.000	0.000	0.000	0.000	0.000	0.000	0.000	0.000	0.000
Mn	0.005	0.006	0.000	0.011	0.000	0.000	0.000	0.000	0.001	0.001	0.000	0.001
Mg	3.370	2.836	3.267	2.720	0.003	0.001	0.000	0.000	0.000	0.000	0.000	0.000
Ca	0.006	0.000	0.000	0.013	0.385	0.435	0.423	0.426	0.006	0.006	0.006	0.005
Na	0.023	0.015	0.006	0.017	0.585	0.550	0.569	0.451	0.231	0.311	0.272	0.217
K	1.814	1.852	1.804	1.803	0.009	0.008	0.007	0.005	0.707	0.626	0.675	0.730
X_{Mg}/ X_{An}/X_K	0.68	0.58	0.67	0.57	0.39	0.44	0.42	0.48	0.66	0.75	0.71	0.77

*Total iron as FeO, Fe^{2+} and Fe^{3+} are calculated by stoichiometric charge balance, X_{Mg}=Mg/ (Mg+Fe^{2+}), X_{An}=Ca/ (Ca+Na+K), X_K=K/(Ca+Na+K), p–peak, s–symplectite, m–matrix.

are medium to coarse–grained and xenoblastic in shape (Fig. 2a, d–e). Symplectitic intergrowth of fine–grained orthopyroxene with biotite and cordierite (Fig. 2b, c) as well as coronal growth of orthopyroxene over the garnet in the matrix of cordierite and plagioclase (Fig. 2f) is also present. The X_{Mg} values obtained for matrix type Opx (0.64–0.54) is higher than the symplectite type (0.53–0.40). The Al content varies from 0.158–0.232 a.p.f.u (Table 1).

Cordierite, with distinctive yellow pleochroic haloes around inclusions of zircon, shows typical polysynthetic and sector twinning (Sample No. 14–4B and 14–6F). It occurs as medium to coarse–grained xenoblasts and - occasionally–partially envelopes garnet and orthopyroxene (Fig. 2a–f). The EPMA data show average low anhydrous sum of oxides ca. 96–97% that suggests presence of fluid

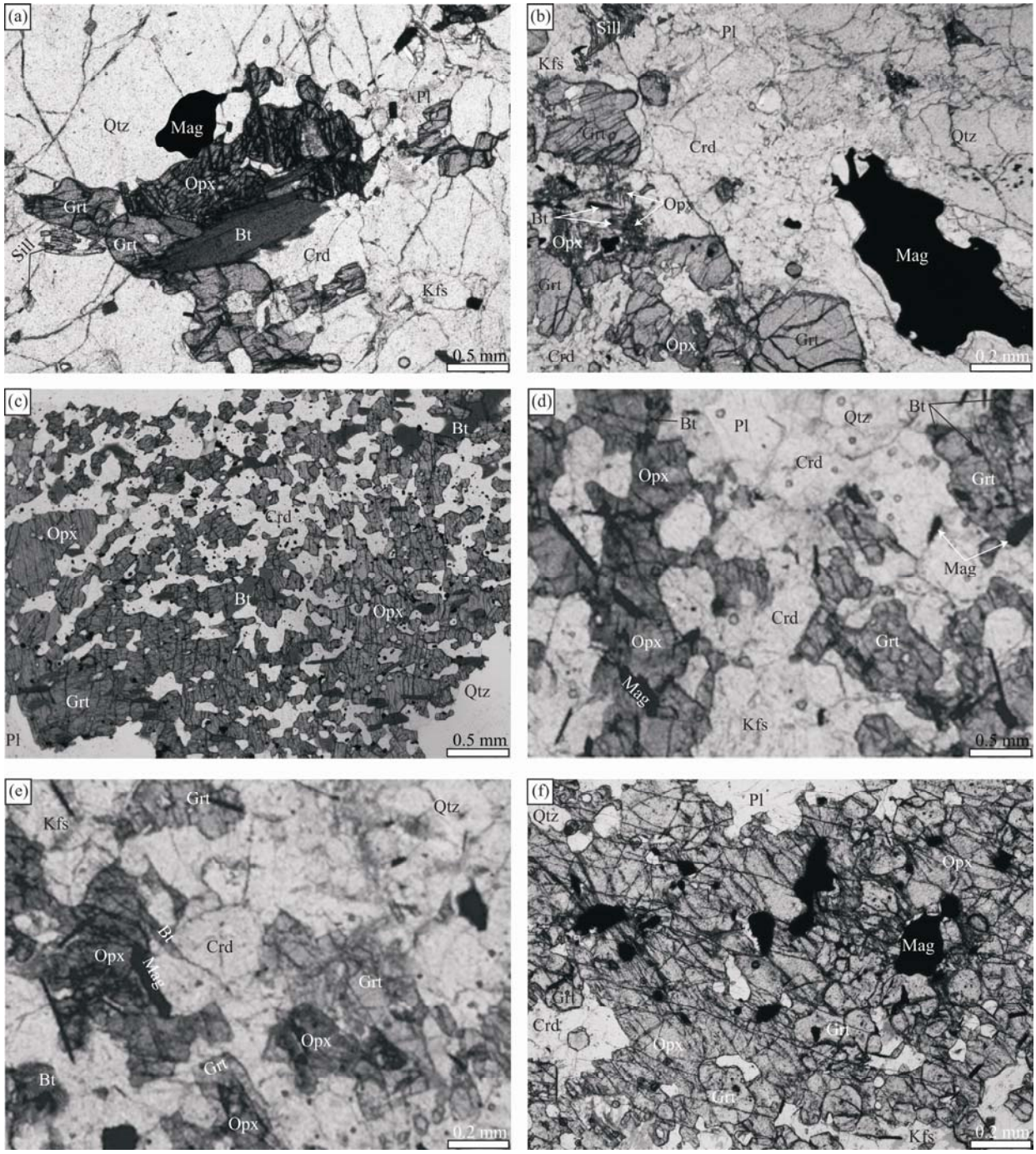

Fig. 2. Microphotographs of garnet–bearing gneiss:
(a) Garnet–orthopyroxene–biotite–cordierite–sillimanite–quartz with magnetite illustrating the peak equilibrium mineral assemblage (ppl, Sample No. 14–4B). Mineral abbreviations were after Kretz (1983). (b) Symplectite intergrowth of the orthopyroxene with cordierite and biotite along the margin of the garnet (ppl, Sample No. 14–4B). (c) Symplectite intergrowth of the orthopyroxene with cordierite and biotite replacing the garnet (ppl, Sample No. 14–4B). (d) Garnet–orthopyroxene–biotite–cordierite–quartz with magnetite illustrating the peak equilibrium mineral assemblage (ppl, Sample No. 14–6F). (e) Garnet is partially replaced with the growth of orthopyroxene and cordierite (ppl, Sample No. 14–6F). (f) Garnet is completely rimmed by the orthopyroxene which is in turn is surrounded by cordierite and plagioclase (ppl, Sample No. 14–6F).

phases about 3–4% in its structural channel. The X_{Mg} values vary from 0.68–0.81 (Table 1).

Biotite flakes are medium to coarse–grained and display characteristic pleochroism from light yellow to dark brown (Fig. 2a–e). Although the main foliation is defined by partially-oriented biotite grains, it is occasionally crosscut by post–kinematic biotite. The early stage biotite is present as inclusions in orthopyroxene and garnet whereas partially enveloped garnet and orthopyroxene with late biotite and biotite–quartz symplectite suggest a retrogation stage. The X_{Mg} values obtained in the biotite of peak assemblage (0.67–0.68) is higher when compared to the decompression assemblage (0.57–0.58). The TiO_2 content varies from 5.15–3.97 wt% (Table 2).

Usually, potash feldspars are medium to coarse–grained (Fig. 2a–b and d–f). Generally, they occur in the form of perthite which includes both crypto (hair) and microperthites. Plagioclase occurs as medium to coarse–grained and contains variable size inclusions of quartz, biotite, magnetite and ilmenite (Fig. 2a–f). The presence of wavy extinction in few grains of potash and plagioclase feldspar signifies the post–crystalline deformation. The X_{An} content of plagioclase is relatively lower (0.39–0.42) in the peak metamorphic assemblage than in the decompression assemblages (0.44–0.48, Table 2). The X_K values vary from 0.66 to 0.77 (Table 2).

Quartz are small to medium–grained xenoblasts and may also be included in garnet as rounded or elongated grains (Fig. 2a–e). Sillimanite occurs as fine to medium–grained needles (Fig. 2a–b). Minor amounts of magnetite, ilmenite, apatite, zircon and rutile occur as accessory minerals. Magnetite, ilmenite and apatite are present as subidioblastic to xenoblastic crystals. Zircon usually occurs as small subidioblastic grains with pleochroic haloes within cordierite and biotite.

4 Metamorphic Conditions

The pressure–temperature (*P–T*), activity of water (X_{H2O}) and oxygen fugacity (fO_2) conditions of the garnet–bearing gneisses have been simultaneously calculated by the 'winTWQ' computer program (version 2.32) of Berman (2007). This program calculates the location of reaction equilibria in pressure–temperature, activity of water and oxygen fugacity ($P–T–X–fO_2$) spaces using the thermodynamic data of Berman (1988, updated 1991, 1996 and December 2006), Berman and Aranovich (1996, updated December 2006) for the end–member phases. Given the offset of end–member phases and a specified P–T window, the program calculates all possible equilibria, both stable and metastable, applicable to that rock. Based on the intersection of all equilibria and a weighting scheme that favours reactions with large volume and entropy changes, the program also calculates a best–fit pressure and temperature for the rock. The results of calculations of the $P–T–X–fO_2$ conditions for both core as well as symplectite compositions of samples 14–4B and 14–6F are shown in Tables 3, 4 and Fig. 3.

4.1 Sample no. 14–4B

The *P–T* estimates obtained with the winTWQ program for the core compositions is 7.1 kbar at 799°C (Fig. 3a), whereas for symplectite compositions it is 4.6 kbar at 784° C (Fig. 3b). The water activity (X_{H2O}) conditions obtained with winTWQ for core and symplectite compositions of garnet–bearing gneisses are 0.14 at 799°C and 7.1 kbar (Fig. 3c), and 0.16 at 784°C and 4.6 kbar (Fig. 4d), respectively. The oxygen fugacity (fO_2) versus temperature calculations at constant pressure yielded the fO_2 values −11.38 and 799°C at 7.1 kbar (Fig. 3e) for the core composition, whereas for the symplectite composition it was −13.05 and 784°C at 4.6 kbar (Fig. 3f).

4.2 Sample no. 14–6F

The core composition yielded the *P–T* condition 6.7 kbar at 807°C (Fig. 3g) and the symplectite composition gave 3.9 kbar at 773°C (Fig. 3h). Water activity against temperature calculations for core and symplectite compositions gave the values of $T–X_{H2O}$ i.e. 807°C and 0.07 at 6.7 kbar (Fig. 3i) and 773°C and 0.11 at 3.9 kbar (Fig. 3j) respectively. The $T–fO_2$ values obtained for both the compositions are 807°C and −11.62 (Fig. 3k) at 6.7 kbar and −14.05 and 773°C at 3.9 kbar (Fig. 3l). It suggests X_{H2O} increased whereas $f(O_2)$ decreased during the decompression stage.

Table 3 Simultaneous calculation of Pressure–Temperature–activity of water and oxygen fugacity conditions at peak and decompression stage (sample no. 14-4B) by the winTWQ program

(a) The P-T conditions obtained by specific equilibria for peak and decompression stage

S. No.	Equilibria plotted in Fig. 1a and b	ΔS(J/M)	ΔV(J/BAR)
1	15Fs + 2Prp + 9Sil = 3Crd + 5Alm	111.16	10.63
2	3Crd = 4Sil + 5Qtz + 2Prp	−108.19	−15.53
3	4Alm + 2Prp + 9Qtz = 12Fs + 3Crd	105.82	19.45
4	3Fs + Sil = Qtz + Alm	0.59	-0.98

(b) The T-X_{H2O} conditions obtained by specific equilibria for peak and decompression stage

S.No.	Equilibria plotted in Fig. 1c and d	ΔS(J/M)	ΔV(J/BAR)
1	4Alm + 2Prp + 9Qtz = 12Fs + 3Crd	105.82	19.45
2	4Alm + 3Kfs + 2Prp+ $3H_2O$ = 3Fs + 3Crd + 3Ann	245.31	24.99
3	4Ann + 3Crd + 3Qtz = 2Prp + 4Kfs + 4Alm + $4H_2O$	−291.80	26.83
4	3Fs + Kfs + H_2O = 3Qtz + Ann	46.50	1.85

(c) The T-fO_2 conditions obtained by specific equilibria for peak and decompression stage

S. No.	Equilibria plotted in Fig. 1e and f	ΔS(J/M)	ΔV(J/BAR)
1	4Alm + 2Prp + 9Qtz = 12Fs + 3Crd	105.82	19.45
2	6Crd + 6Fs + 6Mag = 4Prp + 8Alm + $3O_2$	462.21	−48.96
3	4Alm + 2Prp + $2O_2$= 3Qtz + 4Mag + 3Crd	-343.41	26.16
4	2Mag + 6Qtz = 6Fs + O_2	224.62	−3.35

Table 4 Simultaneous calculation of Pressure–Temperature–activity of water and oxygen fugacity conditions at peak and decompression stage (sample no. 14-6F) by the winTWQ program

(a) The P-T conditions obtained by specific equilibria for peak and decompression stage

S. No.	Equilibria plotted in Fig. 1g and h	ΔS(J/M)	ΔV(J/BAR)
1	4Alm + 2Prp + 9Qtz = 12Fs + 3Crd	105.82	19.45
2	fCrd + 4Fs = 3Qtz + 2Alm	−44.45	−6.74
3	3fCrd + 2Prp = 3Crd + 2Alm	−27.53	−0.77
4	2fCrd + 2Prp + 3Qtz = 4Fs + 3Crd	16.92	5.97

(b) The T-X_{H2O} conditions obtained by specific equilibria for peak and decompression stage

S. No.	Equilibria plotted in Fig. 1i and j	ΔS(J/M)	ΔV(J/BAR)
1	fCrd + 4Fs = 3Qtz + 2Alm	−44.45	−6.74
2	2Alm + Kfs + H_2O = Fs + fCrd + Ann	90.95	8.59
3	6Alm + 4Kfs + $4H_2O$ = 3Qtz + 3fCrd + 4Ann	319.33	27.60
4	3Fs + Kfs + H_2O = 3Qtz + Ann	46.50	1.85

(c) The T-fO_2 conditions obtained by specific equilibria for peak and decompression stage

S. No.	Equilibria plotted in Fig. 1k and l	ΔS(J/M)	ΔV(J/BAR)
1	fCrd + 4Fs = 3Qtz + 2Alm	−44.45	−6.74
2	2fCrd + 2Fs + 2Mag = 4Alm + O_2	135.72	−16.83
3	6Alm + $2O_2$ = 3Qtz + 4Mag + 3fCrd	−315.88	26.93
4	2Mag + 6Qtz = 6Fs + O_2	224.62	−3.35

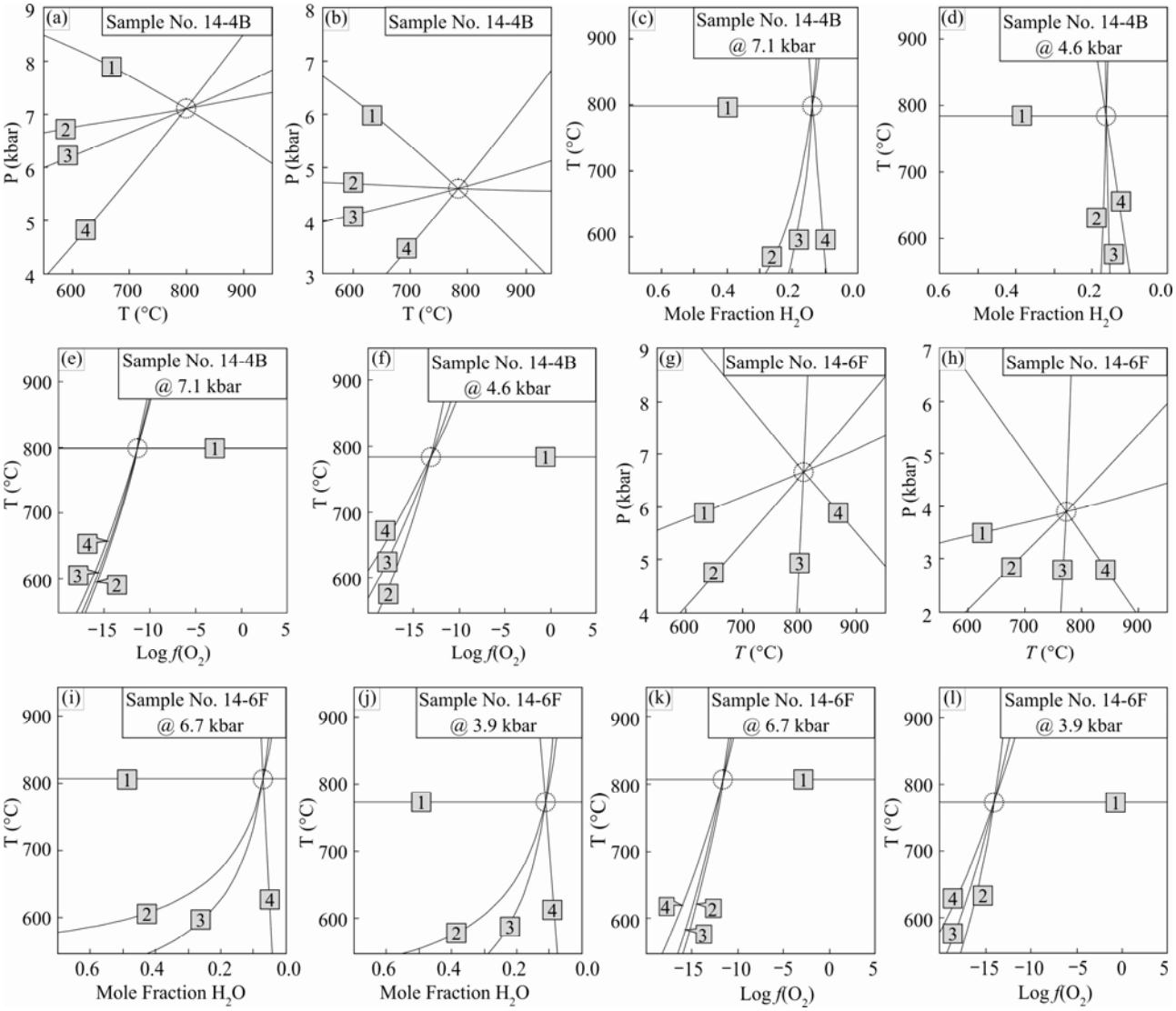

Fig. 3. Results of the simultaneous calculations of Pressure (P)–Temperature (T)–activity of water (X_{H2O}) and oxygen fugacity f (O_2) condition obtained by the winTWQ program with the intersection of specific equilibria for sample No. 14–4B and 14–6F of garnet–bearing gneiss. The specific equilibria are listed in Tables 3 and 4.

5 Discussion

The calculated metamorphic *P–T* conditions clearly indicate an isothermal decompressional path (~3 kbar) experienced by the investigated area (Fig. 4). The lower pressure conditions resulted in the breakdown of corroded garnet and the development of orthopyroxene–cordierite–plagioclase symplectites during decompression. In this study, geothermobarometric estimates suggest that the Karimnagar granulite terrane was buried to depths of nearly c. 24 km. At present, the Eastern Dharwar Craton possesses a crustal thickness of 34–38 km (Borah et al., 2014; Kumar et al., 2014). In view of the existing crustal thickness of ~36 km in the EDC, this suggests that the late Archaean crust was about 60 km thick. Therefore, the garnet–bearing gneiss represents exhumed mid crustal levels, and supports the interpretation of Bohlen and Mezger (1989) that various granulites represent the exposed section of the mid crustal remnant. Although several mechanisms are possible for generating overthickened crust, a clockwise *P–T* path is a likely consequence of concurrent thermal relaxation and erosion following tectonic crustal thickening in a collision belt (England and Thompson, 1984). The production of such an abnormally thick crust could be explained by continental collision and under–thrusting beneath a converging continent. Interpretation of Archaean rock records in terms of modern plate tectonic analogues is sometimes hindered by non–availability of more definitive information on the geological nature of Archaean crust, with special reference to chemical behaviour and isotope data.

Oxidation potential plays a critical role in the stability and appearance of the minerals containing transition metals as well as confining the possible existence and nature of a C–O–H fluid phase in granulite facies metamorphism (Lal et al., 1998; Newton, 1986). Graphite,

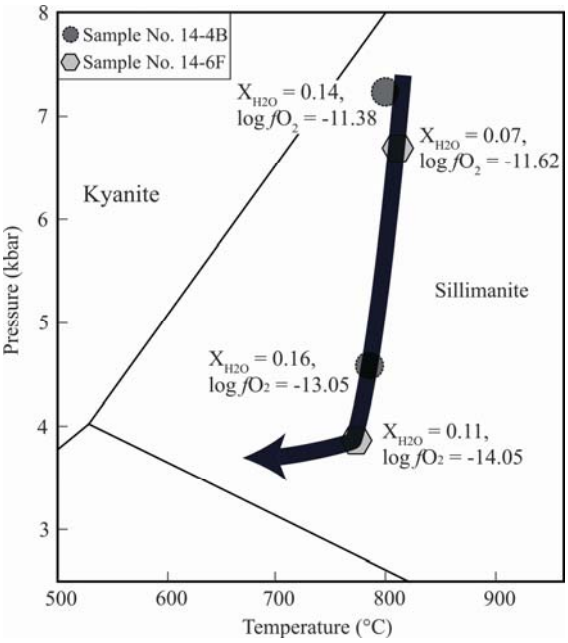

Fig. 4. The pressure–temperature diagram showing the isothermal decompressional *P–T* path for garnet–bearing gneiss of the studied area.

which is one of the oxidation sensitive minerals, is generally present in the granulites of south India. However, graphite is typically absent in the present area, which may be due to the high oxidation conditions (up to −11.38) during the metamorphism and subsequent exhumation of the Karimnagar granulites. The calculated fO_2 values lie above quartz–fayalite–magnetic (QFM) and graphite–carbon dioxide–oxygen (C–O–CO_2) buffers, accounting for the absence of graphite in these granulites (Fig. 5).

The role of water activity in granulite facies metamorphism is an important aspect for discussion. There is no evidence to estimate water activity at the thermal peak as well as prior to granulite facies metamorphism. The segregated lensoid patches of quartzo–feldspathic material and thick veins of quartz in the sapphirine–spinel–bearing granulite, charnockites and mafic granulites are few field evidences which reflect limited partial melting (Prakash et al., 2017). It is very difficult to postulate the time of formation of these quartzo–feldspathic materials. The estimated X_{H2O} based on the almandine, ferrosilite, fe–cordierite, annite, k–feldspar, quartz and water equilibrium and the minimum granite melting curve at variable water activity, prohibits the partial melting condition on a large scale in the granulites of the investigated area. Sapphirine–spinel–corundum–bearing granulites have been reported from the Karimnagar area (Prakash et al., 2013a; Prakash and Singh, 2014). The association of corundum with magnetite–ilmenohematite in the core of the spinel reveals that high fO_2 prevailed either prior to the thermal peak of metamorphism or just before the thermal peak. The fO_2 reduced during the metamorphic evolution and at lower *P–T* conditions. Spinel and sapphirine with ilmenite–hematite intergrowths are rarely observed. The corundum

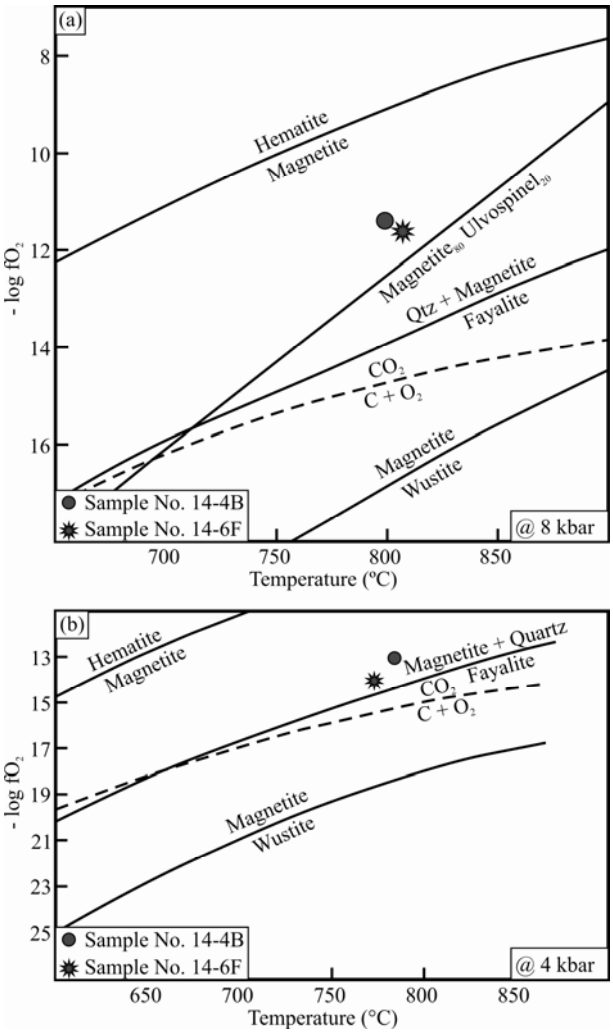

Fig. 5. (a) Estimated oxygen fugacity of the garnet-bearing gneiss at the thermal peak of metamorphism is plotted in log fO_2 (fugacity) vs temperature (°C) at a constant pressure of 8 kbar. Curves of the buffers hematite-magnetite, magnetite–wustite and fayalite + magnetite–quartz have been calculated from the thermodynamic data of Robie et al. (1978) and are consistent with Valley et al. (1990). The curves of the graphite buffer (CO_2–C+O_2) and magnetite$_{80}$ ulvospinel$_{20}$ buffers are taken from Valley et al. (1990). (b) Estimated oxygen fugacity of the late retrograde stage is plotted in a fugacity (- log fO_2) vs temperature and at a constant pressure of 4 kbar. The graphite buffer curve is taken from Newton (1986).

is still incompatible with cordierite and is separated from it by sapphirine and biotite. The absence of the relict igneous textures, exsolution textures, and spinel trellis texture, as well as higher oxygen fugacity and lower X_{H2O} conditions indicate the dominant presence of the high–pressure CO_2 rich fluid during granulite facies metamorphism (Newton, 1986). In the study area, the absence of the above textures and higher oxygen fugacity conditions points to a type of highly CO_2-fluxed granulite facies metamorphism. Similar high fO_2 values are also reported from the granulites of the Eastern Ghats Mobile Belt (Lal et al., 1998) and Southern Granulite terrane

(Prakash, 2000). In the Eastern Ghats granulites and elsewhere, the composition, causes and role of metamorphic fluids have been a matter of debate (Kerrick and Caldeira, 1998; Santosh and Omori, 2008). The transformation of amphibolite facies rocks into granulite facies rocks is now considered to be due to a decrease in water activity and an increase in carbon dioxide in the fluid. Theoretical treatment of melting equilibria under water undersaturated conditions (Wentlandt, 1981; Thompson, 1982; Powell, 1983; Waters, 1988 and others) suggests that formation of the melt would progressively decrease with decreasing aH_2O and allow the activity of water to be locally controlled by the extent of the melting process (Lang and Rice, 1985; Bhattacharya and Sen, 1986). In the second model, infiltration of deep seated CO_2 may dilute H_2O in the fluid phase, which would shift the dehydration reactions towards completion at lower temperatures and possibly remove large–ion lithophile elements (Janardhan et al., 1979; Newton et al., 1980; Lamb and Valley, 1984, Valley et al., 1990; Frost and Frost, 1987).

6 Conclusion

(1) The garnet–bearing gneiss from the Sarvapuram area of the Karimnagar granulites experiences a clockwise *P–T* path with a substantial decompression of 3.0 kbar. The evolution of Karimnagar is related to the subduction and/or collision-related tectonic processes.

(2) The calculated low water activities and high oxidation conditions for peak and decompression stages as well as absence of the relict igneous textures, exsolution textures, and spinel trellis texture suggest highly CO_2-fluxed granulite facies metamorphism. The high log fO_2 values are responsible for the absence of graphite in garnet –bearing gneiss.

(3) It might be ideal to supplement this preliminary study by means of detailed mineralogical and petrological studies in conjunction with the *P–T–X* phase equilibria models and fluid inclusion studies to generate a better scenario for the crustal evolution of the Karimnagar granulite terrane as well as the type of fluids present during the metamorphic history of it.

Acknowledgements

This work has been possible through a Post – Doctoral Fellowship (Indian Institute of Technology, Bombay) and UGC–RFSMS fellowship (Banaras Hindu University) to PCS. We are thankful to the Late Prof. R.K. Lal for his motivational guidance to think this way. We thank two anonymous reviewers for their valuable comments and suggestions, which upgraded significantly a previous draft of the manuscript. Dr. Lian Liu is thanked for his editorial efforts.

Manuscript received Aug. 30, 2018
accepted Dec. 5, 2018
associate EIC HAO Ziguo
edited by Jeff LISTON and FEI Hongcai

Reference

Berman, R.G., 1988. Internally-consistent thermodynamic data for minerals in the system Na_2O-K_2O-CaO-MgO-FeO-Fe_2O_3-Al_2O_3-SiO_2-TiO_2-H_2O-CO_2. Journal of Petrology, 29(2): 445–522.

Berman, R.G., 1991. Thermobarometry using multi-equilibrium calculations; a new technique, with petrological applications. The Canadian Mineralogist, 29(4): 833–855.

Berman, R.G., 2007. winTWQ (version 2.3): a software package for performing internally-consistent thermobarometric calculations. Geological Survey of Canada, open file, 5462: 41.

Berman, R.G., and Aranovich, L. Y., 1996. Optimized standard state and solution properties of minerals. Contributions to Mineralogy and Petrology, 126(1): 1–24.

Bhattacharya, A., and Sen, S.K., 1986. Granulite metamorphism, fluid buffering, and dehydration melting in the Madras charnockites and metapelites. Journal of Petrology, 27: 1119–1141.

Bohlen, S.R., 1987. Pressure-temperature-time paths and a tectonic model for the evolution of granulites. The Journal of Geology, 95(5): 617–632.

Bohlen, S.R., 1991. On the formation of granulites. Journal of Metamorphic Geology, 9(3): 223–229.

Bohlen, S.R., and Mezger, K., 1989. Origin of granulite terranes and the formation of the lowermost continental crust. Science, 244(4902): 326–329.

Borah, K., Rai, S.S., Priestley, K., and Gaur, V.K., 2014. Complex shallow mantle beneath the Dharwar Craton inferred from Rayleigh wave inversion. Geophysical Journal International, 198(2): 1055–1070.

Crowe, W.A., Nash, C.R., Harris, L.B., Leeming, P.M., and Rankin, L.R., 2003. The geology of the Rengali Province: implications for the tectonic development of northern Orissa, India. Journal of Asian Earth Sciences, 21(7): 697–710.

Dasgupta, S., 1995. Pressure-temperature evolutionary history of the Eastern Ghats granulite province: Recent advances and some thoughts. Memoirs-Geological Society of India: 101–110.

England, P.C., and Thompson, A.B., 1984. Pressure-temperature -time paths of regional metamorphism I. Heat transfer during the evolution of regions of thickened continental crust. Journal of Petrology, 25(4): 894–928.

Frost, B.R., and Frost, C.D., 1987. CO_2, melts, and granulite metamorphism. Nature, 327: 503–506.

Gerya, T., 2014. Precambrian geodynamics: Concepts and models. Gondwana Research, 25(2): 442–463.

Harley, S.L., 1989. The origins of granulites: a metamorphic perspective. Geological Magazine, 126(03): 215–247.

Janardhan, A.S., Newton, R.C., and Smith, J.V., 1979. Ancient crustal metamorphism at low P_{H2O}: charnockite formation at Babbaldurga. *Nature*, 278: 511–514.

Kerrick, D.M., and Caldeira, K., 1998. Metamorphic CO_2 degassing from orogenic belts. Chemical Geology, 145(3–4): 213–232.

Kretz, R., 1983. Symbols for rock-forming minerals. American Mineralogist, 68: 277–279.

Kumar, N., Zeyen, H., and Singh, A.P., 2014. 3D lithosphere density structure of southern Indian shield from joint inversion of gravity, geoid and topography data. Journal of Asian Earth Sciences, 89(0): 98–107.

Lal, S.N., Thomas, H., and Prakash, D., 1998. Oxidation condition during granulite metamorphism in Anakapalle area, Eastern ghats belt, India. Proceedings of the Indian National Science Academy - Part A: Physical Sciences, 68(II): 181–184.

Lamb, W.M., and Valley, J.M., 1984. Metamorphism of reduced granulites in low-CO_2; vapour-free environment. Nature, 312: 56–58.

Lang, H.M., and Rice, J.M., 1985. Regression modelling of metamorphic reactions in metapelites, Snow Peak, Northern Idaho. Journal of Petrology, 26(4): 857–887.

Mahabaleswar, B., Jayanand, M., Peucat, J., and Swamy, N.S., 1995. Archaean high-grade gneiss complex from Satnur-Halagur-Sivasamudram areas, Karnataka, southern India:

Petrogenesis and crustal evolution. Journal of the Geological Society of India, 45(1): 33–49.
Maibam, B., Goswami, J.N., and Srinivasan, R., 2011. Pb–Pb zircon ages of Archaean metasediments and gneisses from the Dharwar craton, southern India: Implications for the antiquity of the eastern Dharwar craton. Journal of Earth System Science, 120(4): 643–661.
Mishra, D.C., Singh, B., Tiwari, V.M., Gupta, S.B., and Rao, M.B.S.V., 2000. Two cases of continental collisions and related tectonics during the Proterozoic period in India — insights from gravity modelling constrained by seismic and magnetotelluric studies. Precambrian Research, 99(3): 149–169.
Mohan, A., and Jayananda, M., 1999. Metamorphism and isotopic evolution of granulites of southern India: Reference to Neoproterozoic crustal evolution. Gondwana Research, 2 (2): 251–262.
Naqvi, S. M., and Rogers, J.J.W., 1987. Precambrian geology of India. Oxford University Press.
Newton, R.C., 1986. Fluids of Granulite facies metamorphism fluid-rock interactions during metamorphism, 36–59, Springer New York, New York, NY.
Newton, R.C., Smith, J.V., and Windley, B.F., 1980. Carbonic metamorphism, granulites and crustal growth. Nature, 288: 45 –50.
Patel, S.C., Ravi, S., Kumar, A., and Pati, J.K., 2010. Sapphirine bearing Mg-Al xenolith in Proterozoic kimberlite from Dharwar craton South India. Current Science, 98(4): 547–550.
Peucat, J.-J., Jayananda, M., Chardon, D., Capdevila, R., Fanning, C.M., and Paquette, J.-L., 2013. The lower crust of the Dharwar Craton, Southern India: Patchwork of Archean granulitic domains. Precambrian Research, 227(0): 4–28.
Pichamuthu, C., 1965. Regional metamorphism and charnockitization in Mysore State, India. Indian Mineral, 6: 119–126.
Powell, R., 1983. Processes in granulite-facies metamorphism. In: Atherton, M.P., and Gribble, C.D. (eds,), Migmatites, melting and metamorphism. Shiva, Nantwich, 127–139.
Prakash, D., 2000. Low oxidation condition during granulite metamorphism in Kodaikanal Masiff, south India. Bulletin of the Indian Geologists' Association, 32(2): 19–23.
Prakash, D., Chandra Singh, P., Arima, M., and Singh, T., 2012. P–T history and geochemical characterization of mafic granulites and charnockites from west of Periya, North Kerala, Southern India. Journal of Asian Earth Sciences, 61: 102–115.
Prakash, D., Chandra Singh, P., and Hokada, T., 2013a. A new occurrence of sapphirine-spinel-corundum-bearing granulite from NE of Jagtiyal, Eastern Dharwar Craton, Andhra Pradesh. Journal of the Geological Society of India, 82(1): 5–8.
Prakash, D., Chandra Singh, P., Tewari, S., Joshi, M., Frimmel, H. E., Hokada, T., and Rakotonandrasana, T., 2017. Petrology, pseudosection modelling and U-Pb geochronology of silica-deficient Mg-Al granulites from the Jagtiyal section of Karimnagar granulite terrane, northeastern Dharwar Craton, India. Precambrian Research, 299: 177–194.
Prakash, D., Deepak, Chandra Singh, P., Singh, C.K., Tewari, S., Arima, M., and Frimme, H.E., 2015. Reaction textures and metamorphic evolution of Sapphirine spinel bearing and associated Granulites from Diguva Sonaba, Eastern Ghats Mobile Belt, India. Geological Magazine, 152: 316–340.
Prakash, D., and Sharma, I.N., 2008. Reaction textures and metamorphic evolution of quartz-free granulites from Namlekonda (Karimnagar), Andhra Pradesh, Southern India. International Geology Review, 50(11): 1008–1021.
Prakash, D., and Sharma, I.N., 2011. Metamorphic evolution of the Karimnagar granulite terrane, Eastern Dharwar Craton, south India. Geological Magazine, 148(01): 112–132.
Prakash, D., Singh, C.K., Chandra Singh, P., Deepak, and Kumar, A., 2011. GIS based terrain modelling of the area NW of Karimnagar, Southern India. International Journal of Remote Sensing Applications, 1(2): 6–10.
Prakash, D., Singh, C.K., Shukla, U.K., Chandra Singh, P., Singh, A., and Chandra, A., 2013b. Structural and geomorphological evolution of the area around Narella, Andhra Pradesh, India: A study based on field investigation, GIS and remote sensing. International Journal of Remote Sensing Applications, 3(1): 24–32.
Prakash, D., and Singh, P.C., 2014. New finding of sillmanite in sapphirine-bearing granulites from Pedapalli, NE part of the Eastern Dharwar Craton, India. Journal of the Geological Society of India, 84(1): 29–34.
Raase, P., Raith, M., Ackermand, D., and Lal, R., 1986. Progressive metamorphism of mafic rocks from greenschist to granulite facies in the Dharwar Craton of South India. The Journal of Geology, 94(2): 261–282.
Raith, M., Raase, P., Ackermand, D., and Lal, R., 1982. The Archean craton of southern India: metamorphic evolution and PT Conditions. Geologische Rundschau, 71(1): 280–290.
Robie, R.A., Hemingway, B.S., and Fisher, J.R., 1978. Thermodynamic properties of minerals and related substances at 298.15 K and 1 bar (10^5 Pascals) pressure and at higher temperatures. U.S. Geological Survey Bulletine, 1452.
Santosh, M., and Omori, S., 2008. CO_2 flushing: a plate tectonic perspective. Gondwana Research, 13: 86–102.
Sarbajna, C., Bose, S., Rajagopalan, V., Das, K., Som, A., Paul, A.K., Shivkumar, K., Umamaheswar, K., and Chaki, A., 2013. U–Cr-rich high Mg-Al granulites from Karimnagar Granulite Belt, India: implications for Neoarchean-Paleoproterozoic events in southern India. Mineralogy and Petrology, 107(4): 553–571.
Sharma, I.N., and Prakash, D., 2008. A new occurrence of sapphirine-bearing granulite from Podur, Andhra Pradesh, India. Mineralogy and Petrology, 92(3–4): 415–425.
Sizova, E., Gerya, T., and Brown, M., 2014. Contrasting styles of Phanerozoic and Precambrian continental collision. Gondwana Research, 25(2): 522–545.
Spear, F.S., 1992. Thermobarometry and PT paths from granulite facies rocks: an introduction. Precambrian Research, 55(1–4): 201–207.
Spear, F.S., 1993. Metamorphic Phase Equilibria and Pressure-Temperature-Time Paths, Book Crafters. Inc., Chelsea, Michigan, USA, 70.
Thompson, A.B., 1982. Dehydration melting of pelitic rocks and the generation of H_2O-undersaturated granitic liquids. American Journal of Science, 282(10): 1567–1595.
Valley, J.W., Bohlen, S.R., Essene, E.J., and Lamb, W., 1990. Metamorphism in the adirondacks: II. The role of fluids. Journal of Petrology, 31: 555–596.
Waters, D.J., 1988. Partial melting and the formation of granulite facies assemblages in Namaqualand, South Africa. Journal of Metamorphic Geology, 6: 387–404.
Wentlandt, R.F., 1981. Influence of CO_2 on melting of model granulite facies assemblages: a model for the genesis of charnockites. American Mineralogist, 66: 1164–1174.
Zhai, M., Guo, J., and Liu, W., 2005. Neoarchean to Paleoproterozoic continental evolution and tectonic history of the North China Craton: a review. Journal of Asian Earth Sciences, 24(5): 547–561.

About the first and corresponding author

Dr. P. Chandra SINGH is a Postdoc Fellow at the Department of Earth Sciences, Indian Institute of Technology Bombay (India). He received his B.Sc. (Hons.) and M.Sc. degree in Geology from Banaras Hindu University, India. He earned his doctorate degree in geology from the Department of Geology, Banaras Hindu University (India) in 2015. His work is focused to understand tectono-metamorphic evolution of the polymetamorphic terranes of India using the multidisciplinary approach e.g., field relations, reaction micro-textures, evolution of mineral assemblages, high-resolution geochemical analyses, thermobarometric calculations, equilibrium thermodynamics, and U-Pb dating of the minerals (zircon, monazite) or mineral zones to constrain the time component of different metamorphic stages. He has received CSIR- NET award in 2009 and UGC RFSMS award in 2010.